INTERNATIONAL JOURNAL FOR NUMERICAL METHODS IN FLUIDS
Int. J. Numer. Meth. Fluids 2005; **48**:349–366
Published online 21 January 2005 in Wiley InterScience (www.interscience.wiley.com). DOI: 10.1002/fld.895

2D thermal/isothermal incompressible viscous flows

Alfredo Nicolás[1,*,†] and Blanca Bermúdez[2]

[1]*Depto. Matemáticas, 3er. Piso Ed. AT-Diego Bricio, UAM-Iztapalapa, 09340 México D.F., México*
[2]*Facultad de C. de la Computación, BUAP, Pue., México*

SUMMARY

2D thermal and isothermal time-dependent incompressible viscous flows are presented in rectangular domains governed by the Boussinesq approximation and Navier–Stokes equations in the stream function–vorticity formulation. The results are obtained with a simple numerical scheme based on a fixed point iterative process applied to the non-linear elliptic systems that result after a second-order time discretization. The iterative process leads to the solution of uncoupled, well-conditioned, symmetric linear elliptic problems. Thermal and isothermal examples are associated with the unregularized, driven cavity problem and correspond to several aspect ratios of the cavity. Some results are presented as validation examples and others, to the best of our knowledge, are reported for the first time. The parameters involved in the numerical experiments are the Reynolds number *Re*, the Grashof number *Gr* and the aspect ratio. All the results shown correspond to steady state flows obtained from the unsteady problem. Copyright © 2005 John Wiley & Sons, Ltd.

KEY WORDS: fixed point iterative process; Reynolds and Grashof numbers; mixed convection; rectangular domains

1. INTRODUCTION

In this paper, 2D mixed convection and isothermal incompressible viscous flows are presented in rectangular domains governed by the Boussinesq approximation and Navier–Stokes equations; the governing equations are in terms of the stream function–vorticity variables. The results are obtained with a simple numerical scheme based on a fixed point iterative process applied to the non-linear systems that result after a convenient second-order time discretization is made. The iterative process leads to the solution of uncoupled, well-conditioned, symmetric linear elliptic problems for which, as is well-known, very efficient solvers exist regardless of the space discretization.

The numerical scheme is an extension of one developed for isothermal problems reported in Reference [1]. Because of the simplicity of the scheme and the good conditioning of the

*Correspondence to: Alfredo Nicolás, Depto. Matemáticas, 3er. Piso Ed. AT-Diego Bricio, UAM-Iztapalapa, 09340 México D.F., México.
†E-mail: anc@xanum.uam.mx

Received 3 October 2003
Revised 9 November 2004
Accepted 10 November 2004

resultant algebraic linear systems, no upwinding ingredient is used; fine meshes can be handled without too much computational effort in medium computers when convection dominance or large force terms are involved, and an iterative method like cyclic reduction is used.

The numerical experiments take place in rectangular domains associated with the well-known, unregularized driven cavity problem which implies re-circulation phenomena because of its velocity boundary condition. The flow parameters involved are the Reynolds number Re, the Grashof number Gr and the aspect ratio of the domain (ratio of the height to the width). In this regard, results with different aspect ratios are presented for isothermal flows with Reynolds number $Re = 1000$ and non-isothermal mixed convection ones with Reynolds number $400 \leqslant Re \leqslant 3000$ and Grashof numbers $10^2 \leqslant Gr \leqslant 10^7$. Some of the results are presented as validation of the method, while others are new results which, to our knowledge, are reported for the first time. Our aim is to describe the nature of the flows, mainly on the new ones, rather than to analyse the numerical algorithm.

However, to support the validation of the results, mesh size and time-step independence studies are carried out. Computations are made on a fixed mesh size with different time steps, on different mesh sizes with fixed time step, and a combination of both (mesh size and time step) since finer meshes lead necessarily to a reduction in the time step due to stability requirements, an issue not discussed here. The discrepancies are measured in terms of the relative L_∞ discrete norm and the max/min values of the stream function ψ.

The new results show that the flows have a strong dependence on the aspect ratio, the Reynolds number Re and the Grashof number Gr: the number of cells for the streamlines increases as either the aspect ratio, Re, or Gr increases, and the isotherms tend to spread into the whole cavity, at least for the contour values considered; the final time where the steady state is reached increases also according to this dependence.

By definition, a *steady state* (or stationary) *flow* is a flow where the velocity $\mathbf{u}$ (equivalently, the vorticity ω in stream function–vorticity variables) is independent of time at any spatial point occupied by the fluid [2, 3] implying no contribution of the time derivative in the momentum equations. By solving unsteady problems, one has to decide the goal to reach. In this work, all the results shown correspond to steady state flows obtained from the unsteady problem, which means that the flows are the converged asymptotic steady state, independent of time, obtained as time t approaches $+\infty$ (large time, in practice). That is, at this stage, no time-dependent flow is under study since no sufficiently large Reynolds number Re is considered [4].

Previous work, reported partially in Reference [5], has already been done to validate the scheme for natural convection flows in a unit square cavity. For natural convection flows the cavity is bounded by rigid and fixed walls, whereas for mixed convection the top wall is in motion (implied by the driven cavity problem). As a consequence, the latter flows are more difficult to handle; the results shown here illustrate the robustness of the scheme.

It is known that the limitation of the stream function–vorticity formulation makes it less desirable than the generality of the primitive variables formulation. However, recent experiments in rectangular cavities with the numerical scheme in Reference [6] in primitive variables, even though the meshes are coarser due to an upwinding stabilization process, show that the simplicity of the method employed here, in stream function–vorticity variables, has a superior efficiency.

Hereafter, the paper is organized in sections as follows: Section 2—Continuous Problem; Section 3—Numerical Scheme; Section 4—Numerical results; Section 5—Conclusions.

2. CONTINUOUS PROBLEM

Let $\Omega \subset R^N (N = 2, 3)$ be the region of the unsteady flow of a non-isothermal incompressible viscous fluid, and Γ its boundary. Under the well-known Boussinesq approximation, this kind of time-dependent flow is governed by the non-dimensional equations given by

$$\mathbf{u}_t - \frac{1}{Re}\Delta\mathbf{u} + \nabla p + (\mathbf{u}\cdot\nabla)\mathbf{u} = \frac{G_r}{Re^2}\theta\mathbf{e} \quad \text{in } \Omega,\ t>0 \tag{1a}$$

$$\nabla\cdot\mathbf{u} = 0 \quad \text{in } \Omega,\ t>0 \tag{1b}$$

$$\theta_t - \frac{1}{RePr}\Delta\theta + \mathbf{u}\cdot\nabla\theta = 0 \quad \text{in } \Omega,\ t>0 \tag{1c}$$

where $\mathbf{u}$, p and θ are the velocity, pressure and temperature of the flow, respectively. The parameters Re, Gr and Pr are the Reynolds, Grashof and Prandtl numbers, respectively, and $\mathbf{e}$ is the unit vector in the direction of the gravitational force.

Remark
The pure isothermal case, known as the Navier–Stokes equations, is a particular case of (1a)–(1c): there is no coupling with the thermal energy equation (1c) and only the momentum equation (1a) and the incompressibility constraint (1b) are considered, and the right-hand side in (1a) involves a concentration of external forces $\mathbf{f}$ independent of θ, and therefore, independent of the parameters Gr and Re.

The momentum equation (1a) and the temperature equation (1c) should be supplemented with appropriate initial conditions

$$\mathbf{u}(\mathbf{x}, 0) = \mathbf{u}_0(\mathbf{x}) \quad \text{in } \Omega \quad (\nabla\cdot\mathbf{u}_0 = 0) \tag{2a}$$

$$\theta(\mathbf{x}, 0) = \theta_0(\mathbf{x}) \quad \text{in } \Omega \tag{2b}$$

and boundary conditions, say for instance

$$\mathbf{u} = \mathbf{f}_1 \quad \text{on } \Gamma,\ t\geqslant 0 \quad \left(\int_\Gamma \mathbf{f}_1\cdot\mathbf{n}\,\mathrm{d}\Gamma = 0\right) \tag{3a}$$

$$B\theta = 0 \quad \text{on } \Gamma,\ t\geqslant 0 \tag{3b}$$

where B is a boundary operator for θ, which can involve Dirichlet, Neumann or mixed boundary conditions.

Restricting the domain for equations (1a)–(1c) to the 2D case, taking the *curl* on both sides of (1a) and taking into account the relations

$$u_1 = \frac{\partial\psi}{\partial y}, \quad u_2 = -\frac{\partial\psi}{\partial x} \tag{4}$$

where $(u_1, u_2) = \mathbf{u}$ and ψ is the stream function, the component in the $\mathbf{k} = (0, 0, 1)$ direction gives the system of scalar equations

$$\Delta\psi = -\omega \quad \text{in } \Omega, \ t > 0 \tag{5a}$$

$$\omega_t - \nu\Delta\omega + \mathbf{u} \cdot \nabla\omega = \frac{G_r}{Re^2} \frac{\partial\theta}{\partial x} \quad \text{in } \Omega, \ t > 0 \tag{5b}$$

$$\theta_t - \frac{1}{RePr} \Delta\theta + \mathbf{u} \cdot \nabla\theta = 0 \quad \text{in } \Omega, \ t > 0 \tag{5c}$$

where $1/Re$ has been replaced by the viscosity parameter ν, and ω is the vorticity, which, from $\omega\mathbf{k} = \nabla \times \mathbf{u} = -\Delta\psi\mathbf{k}$, is given by

$$\omega = \frac{\partial u_2}{\partial x} - \frac{\partial u_1}{\partial y} \tag{6}$$

System (5a)–(5c) are the corresponding Boussinesq equations in stream function–vorticity variables associated with the ones in primitive variables (1a)–(1c). Analogous to the primitive variables formulation, if the right-hand side of (5b) is given by a function of external forces $\mathbf{f}$, independent of θ, and there is no coupling with the thermal energy equation (5c), the corresponding system (5a)–(5b) gives the Navier–Stokes equations in stream function–vorticity variables. It should be noted that because of the relations in (4) the incompressibility condition (1b) is satisfied automatically in Ω, which is a significant advantage. The disadvantage is that there is no boundary condition given for vorticity. As mentioned in References [7, 8], ψ is over-determined on the boundary ($\frac{\partial\psi}{\partial n}|_\Gamma$ is also known) but no boundary condition is given for ω. Actually, in Reference [7] a procedure is given to obtain the boundary condition for ω in general domains.

This work is only concerned with 2D rectangular domains, and therefore Equations (5a)–(5c) are set in the domain $\Omega = (0, a) \times (0, b)$ with $a, b > 0$. The motion boundary condition, in terms of the primitive variable $\mathbf{u}$, is defined by: (a) *Isothermal* case: $\mathbf{u} = (1, 0)$ at the moving boundary (the top one $y = b$) and $\mathbf{u} = (0, 0)$ elsewhere; as is well-known, this kind of boundary condition corresponds to the unregularized, driven cavity problem, mostly given for the unit square but in Reference [9], for instance, where a cavity of aspect ratio 2 is considered. (b) *Mixed convection*: the same as in the isothermal case for velocity and the boundary condition for the temperature θ is still given implicitly by the operator B in (3b); it will be given explicitly in Section 4.

A brief discussion for the translation of the boundary condition in terms of the velocity primitive variable $\mathbf{u}$ to the ψ–ω variables follows; the discussion is given for the isothermal case only since this situation trivially implies the corresponding one for mixed convection. Following Reference [1] (see also Reference [9]), by (4), ψ is a constant function on rigid and fixed walls; at the moving wall $y = b$, a constant function for ψ is also obtained, then $\psi = 0$ is chosen on Γ. By Taylor expansion of (5a) on the boundary, with h_x and h_y the space

steps, one obtains

$$\begin{aligned}
\omega(0,y,t) &= -\frac{1}{2h_x^2}[8\psi(h_x,y,t) - \psi(2h_x,y,t)] + O(h_x^2)\\
\omega(a,y,t) &= -\frac{1}{2h_x^2}[8\psi(a-h_x,y,t) - \psi(a-2h_x,y,t)] + O(h_x^2)\\
\omega(x,0,t) &= -\frac{1}{2h_y^2}[8\psi(x,h_y,t) - \psi(x,2h_y,t)] + O(h_y^2)\\
\omega(x,b,t) &= -\frac{1}{2h_y^2}[8\psi(x,b-h_y,t) - \psi(x,b-2h_y,t)] - \frac{3}{h_y} + O(h_y^2)
\end{aligned} \tag{7}$$

In addition, $\omega(\mathbf{x},0)=\omega_0(\mathbf{x})$ and $\theta(\mathbf{x},0)=\theta_0(\mathbf{x})$ denote the initial conditions for the vorticity and for the temperature, respectively; the initial vorticity, by (6) has to satisfy $\omega_0=\partial u_{02}/\partial x - \partial u_{01}/\partial y$ if $\mathbf{u_0}=(u_{01},u_{02})$ is the initial velocity.

3. NUMERICAL SCHEME

About time discretization, ω_t and θ_t appearing in the (5b) and in (5c), respectively, are approximated by the second-order scheme

$$f_t(\mathbf{x},(n+1)\Delta t) = \frac{3f^{n+1} - 4f^n + f^{n-1}}{2\Delta t}, \quad n \geqslant 1, \ \ \mathbf{x}\,\varepsilon\,\Omega \tag{8}$$

where Δt denotes the time step and $f^r \equiv f(\mathbf{x}, r\Delta t)$ for a smooth enough function f.

The resulting time discretization system reads

$$\begin{aligned}
\Delta\psi^{n+1} &= -\omega^{n+1} \quad \text{in } \Omega\\
\alpha\omega^{n+1} - \nu\Delta\omega^{n+1} + \mathbf{u}^{n+1}\cdot\nabla\omega^{n+1} &= \frac{G_r}{Re^2}\frac{\partial\theta^{n+1}}{\partial x} + f_\omega, \quad n\geqslant 1 \quad \text{in } \Omega\\
\alpha\theta^{n+1} - \frac{1}{RePr}\Delta\theta^{n+1} + \mathbf{u}^{n+1}\cdot\nabla\theta^{n+1} &= f_\theta, \quad n\geqslant 1 \quad \text{in } \Omega
\end{aligned} \tag{9}$$

where $\alpha = 3/2\Delta t$, $f_\omega = (4\omega^n - \omega^{n-1})/2\Delta t$, $f_\theta = (4\theta^n - \theta^{n-1})/2\Delta t$, and the components u_1 and u_2 of $\mathbf{u}$, in terms of ψ, are given by (4).

Then, at each time step, a non-linear system of elliptic equations of the following form has to be solved:

$$\begin{aligned}
\Delta\psi &= -\omega \quad \text{in } \Omega, \ \ \psi = 0 \quad \text{on } \Gamma\\
\alpha\omega - \nu\Delta\omega + \mathbf{u}\cdot\nabla\omega &= \frac{G_r}{Re^2}\frac{\partial\theta}{\partial x} + f_\omega \quad \text{in } \Omega, \ \ \omega = \omega_{\text{bc}} \quad \text{on } \Gamma\\
\alpha\theta - \frac{1}{RePr}\Delta\theta + \mathbf{u}\cdot\nabla\theta &= f_\theta \quad \text{in } \Omega, \ \ B\theta = 0 \quad \text{on } \Gamma
\end{aligned} \tag{10}$$

where ω_{bc} denotes the boundary condition for ω given by (7). To obtain $(\psi^1,\omega^1,\theta^1)$ in (9) various second-order strategies can be used by applying an Euler first-order approximation

for the time derivative. For instance: (1) through a sequence of solutions with a smaller time step or (2) computing $(\psi_1, \omega_1, \theta_1)$ with Δt, then, $(\psi_2, \omega_2, \theta_2)$ with $\Delta t/2$, and then taking $(\psi^1, \omega^1, \theta^1) = 2(\psi_2, \omega_2, \theta_2) - (\psi_1, \omega_1, \theta_1)$. In either situation, a system of the form (10) is also obtained.

Taking into account that the elliptic system (10), in addition to being non-linear, is of the non-potential (or transport) type, a fixed point iterative process is used for the solution. This process is similar to one applied previously to mixed convection problems in primitive variables [6]. A distinctive aspect here is that the iterative process is extended up to the boundary to handle the ω boundary conditions given implicitly by unknown interior values of ψ in (7).

Denoting

$$R_\omega(\omega, \psi) \equiv \alpha\omega - \nu\Delta\omega + \mathbf{u} \cdot \nabla\omega - \frac{G_r}{Re^2} \frac{\partial\theta}{\partial x} - f_\omega \quad \text{in } \Omega$$

$$R_\theta(\theta, \psi) \equiv \alpha\theta - \beta\Delta\theta + \mathbf{u} \cdot \nabla\theta - f_\theta \quad \text{in } \Omega$$

where $\beta = 1/RePr$. System (10) is equivalent to

$$\begin{aligned} \Delta\psi &= -\omega \quad \text{in } \Omega, \ \psi = 0 \quad \text{on } \Gamma \\ R_\theta(\theta, \psi) &= 0 \quad \text{in } \Omega, \ B\theta = 0 \quad \text{on } \Gamma \\ R_\omega(\omega, \psi) &= 0 \quad \text{in } \Omega, \ \omega = \omega_{\text{bc}} \quad \text{on } \Gamma \end{aligned} \tag{11}$$

Then, (11) is solved, at time level $(n+1)$, by the fixed point iterative process: *With* $\{\theta^0, \omega^0\} = \{\theta^n, \omega^n\}$ *given, solve until convergence on* θ *and* ω

$$\begin{aligned} \Delta\psi^{m+1} &= -\omega^m \quad \text{in } \Omega, \ \psi^{m+1} = 0 \quad \text{on } \Gamma \\ \theta^{m+1} &= \theta^m - \rho_\theta(\alpha I - \beta\Delta)^{-1} R_\theta(\theta^m, \psi^{m+1}) \quad \text{in } \Omega, \quad B\theta^{m+1} = 0 \quad \text{on } \Gamma, \ \rho_\theta > 0 \\ \omega^{m+1} &= \omega^m - \rho_\omega(\alpha I - \nu\Delta)^{-1} R_\omega(\omega^m, \psi^{m+1}) \quad \text{in } \Omega, \quad \omega^{m+1} = \omega_{\text{bc}}^{m+1} \quad \text{on } \Gamma, \ \rho_\omega > 0 \end{aligned} \tag{12}$$

and then, take $(\omega^{n+1}, \psi^{n+1}, \theta^{n+1}) = (\omega^{m+1}, \psi^{m+1}, \theta^{m+1})$.

Finally, system (12), with the corresponding $\{\theta^0, \omega^0\}$, is equivalent to

$$\begin{aligned} \Delta\psi^{m+1} &= -\omega^m \quad \text{in } \Omega, \quad \psi^{m+1} = 0 \quad \text{on } \Gamma \\ (\alpha I - \beta\Delta)\theta^{m+1} &= (\alpha I - \beta\Delta)\theta^m - \rho_\theta R_\theta(\theta^m, \psi^{m+1}) \quad \text{in } \Omega, \ \rho_\theta > 0 \\ B\theta^{m+1} &= 0 \quad \text{on } \Gamma \\ (\alpha I - \nu\Delta)\omega^{m+1} &= (\alpha I - \nu\Delta)\omega^m - \rho_\omega R_\omega(\omega^m, \psi^{m+1}) \quad \text{in } \Omega, \ \rho_\omega > 0 \\ \omega^{m+1} &= \omega_{\text{bc}} \quad \text{on } \Gamma \end{aligned} \tag{13}$$

It turns out that *three* uncoupled, elliptic linear problems associated with the operators Δ (or $-\Delta$), $\alpha I - \beta\Delta$ and $\alpha I - \nu\Delta$ are solved; for isothermal problems, only *two* of such problems are solved, the ones associated with Δ (or $-\Delta$) and $\alpha I - \nu\Delta$. It should be noted that the non-symmetric parts of θ and ω have been taken to the right-hand side as part of the iterative

process. Therefore, the solution of the original system, at each iteration of each time level, leads to the solution of standard symmetric linear elliptic problems.

It is well-known that for the spatial discretization of elliptic problems like those in (13), either finite differences or finite elements may be used, as far as rectangular domains are concerned; it is also known that in either case very efficient solvers exist. In the finite element case, variational formulations have to be chosen and then restricted to the finite-dimensional finite elements spaces, like for instance those in References [7, 10, 11]. For the specific results in the following section, the second-order approximation of the Fishpack solver [12] has been used, where the algebraic linear systems are solved through an efficient cyclic reduction iterative method [13]. Then, such second-order approximations in space combined with the second-order one for the vorticity boundary condition (7); the centred second-order approximation for $\partial\psi/\partial y$ and $\partial\psi/\partial x$ to get u_1 and u_2 in (4), and $\partial\theta/\partial x$, say in (10); the second-order approximation for the Neumann temperature boundary condition, based on (8); and the second-order approximation in time (8) imply that the whole approximate problem relies on second-order discretizations. It is known that if finite elements are used, all the second-order spatial discretizations can be obtained with linear finite elements; a procedure like the one in Reference [7] is required for (7) to retain second-order accuracy.

4. NUMERICAL RESULTS

As mentioned before, the numerical experiments take place in rectangular domains $\Omega = (0, a) \times (0, b)$, $a, b > 0$, in connection with the unregularized, driven cavity problem. Then, it is to be remembered that the boundary condition of the ψ–ω motion is given by $\psi = 0$ everywhere on the boundary for ψ and by (7) for ω. The initial condition for ω and θ are identically 0. The Prandtl number Pr appearing in the temperature equation (5c) is kept fixed, $Pr = 0.72$, in the numerical experiments for mixed convection. The numerical experiments involve in general Reynolds numbers $400 \leqslant Re \leqslant 3000$; Grashof numbers $100 \leqslant Gr \leqslant 10^7$ in mixed convection thermal problems, and mainly $Re = 1000$ in isothermal ones. The space steps are denoted by h_x, h_y and the time step by Δt.

As stated in the Introduction, all the results shown correspond to steady state flows obtained from the unsteady problem. They are the converged asymptotic steady state obtained as time t approaches $+\infty$ (large time, in practice). To reach convergence to an asymptotic steady state one has to give a stopping criterion for the final time T_{ss} when it is reached; that is, T_{ss} is the time when the solution does not change any longer with respect to time. For mixed convection problems, which are more difficult than isothermal ones, T_{ss} is determined mainly according to the point-wise discrete L_∞ absolute criterion, given later on in (15).

In rectangular cavities, the smallest length of the aspect ratio that works for the corresponding case in a square domain gives a guide for the optimal mesh size for the largest length. For instance, for $Re = 1000$, in a rectangular cavity of aspect ratio 2 the mesh $(h_x, h_y) = (1/120, 2/240)$ is used since the correct result in the unit square cavity, for isothermal and mixed convection problems, is obtained on a mesh $(h_x, h_y) = (1/120, 1/120)$. However, through a mesh independence study, it will be observed that this rule is more demanding with mesh refinement as the aspect ratio increases. For all the results reported, the time step ranges from $\Delta t = 0.02$ to $\Delta t = 0.001$; it will also be observed that Δt has to decrease, due to stability, as mesh refinement is demanded by high aspect ratios.

To support the assumption that the new results are correct, a mesh size and time step independence studies are made in terms of the point-wise discrete L_∞ relative error in the closure $\overline{\Omega}$ of the cavity

$$\begin{aligned} \Delta t \text{ fixed}: & \quad \frac{\|f_{hx1,hy1;\Delta t} - f_{hx2,hy2;\Delta t}\|_\infty}{\|f_{hx1,hy1;\Delta t}\|_\infty} \\ \{h_x, h_y\} \text{ fixed}: & \quad \frac{\|f_{hx,hy;\Delta t1} - f_{hx,hy;\Delta t2}\|_\infty}{\|f_{hx,hy;\Delta t1}\|_\infty} \end{aligned} \tag{14}$$

In connection with this, Iwatsu *et al.* [14], without mentioning explicitly the metric used (but in any case, it has to be an equivalent finite-dimensional one), use only three time steps and three meshes for their mixed convection results in the square cavity. They claim to obtain discrepancies less than 1%, and it is not clear if they are computing their measure in all the cavities as we do. However, for rectangular cavities, things are more difficult and more combinations have to be considered. The above metric is also complemented with the max/min values of the stream function ψ in $\overline{\Omega}$.

It should be clearly understood that to get flow solutions in rectangular cavities, work was first undertaken to obtain correct solutions in the square cavity. In this regard, the validation for the isothermal flow at $Re = 1000$ is given in Reference [1], on a mesh $(h_x, h_y) = (1/120, 1/120)$ with $\Delta t = 0.01$; as can be seen, the validation of some thermal flows is presented in Section 4.2. During this process, numerical experiments were made to see that coarser meshes than $(h_x, h_y) = (1/120, 1/120)$ do not give the correct flows; in connection with this, Goyon [9] obtains results on $(h_x, h_y) = (1/128, 1/128)$. On coarser meshes, the vorticity fails to be correct. This was also tested with the $Re = 400$ flow which cannot be obtained on a mesh coarser than $(h_x, h_y) = (1/80, 1/80)$. Similar experiments were made for the non-isothermal problems. In this case, even though coarse mesh solutions for the streamlines and isotherms may agree with results widely known to be correct, the mesh chosen is the one where the vorticity (not shown) also agrees with the analogous Reynolds number in the isothermal case, as mentioned previously.

Based on the above discussion, the mesh independence study for rectangular cavities considers only mesh sizes smaller or equal to the correct ones used for square cavities, otherwise an evident error may be accumulated.

4.1. Isothermal flows

Figures 1 and 2 show the flows for Reynolds number $Re = 1000$ with aspect ratios 2 and 3 on meshes $(h_x, h_y) = (1/120, 2/240)$, with $\Delta t = 0.01$, and $(h_x, h_y) = (1/320, 3/960)$, with $\Delta t = 0.0025$, respectively. The left contours are the streamlines and the right ones the vorticity contours. The result of Figure 1 agrees very well with the one shown by Goyon [9], on a mesh $(h_x, h_y) = (1/128, 2/256)$ and time step $\Delta t = 0.005$, using a different method; Goyon does not show a result with aspect ratio 3. The contour values are the ones used by Goyon in its aspect ratio 2 result, which in turn are the same in Reference [15] in the square cavity.

To validate the aspect ratio 3 result, computations were made with a set of 4 mesh sizes and different time steps:

(1) mesh size fixed, $(h_x, h_y) = (1/160, 3/480)$, $\{\Delta t\} = \{0.01, 0.005, 0.0025\}$;
(2) time step fixed, $\Delta t = 0.005$, $\{(h_x, h_y)\} = \{(1/160, 3/480), (1/240, 3/720)\}$;

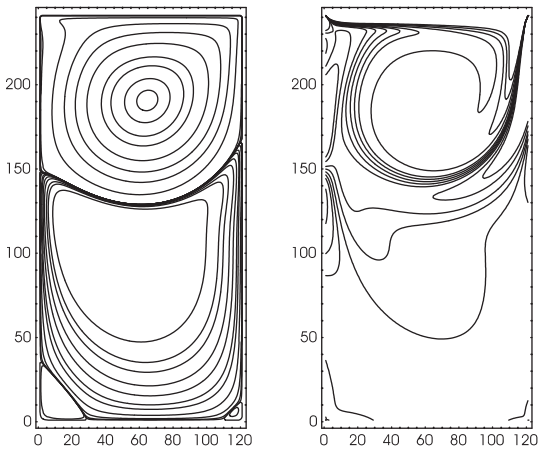

Figure 1. $Re = 1000$; A. ratio 2: $h_x = 1/120$, $h_y = 2/240$: (a) Streamlines; and (b) vorticity contours.

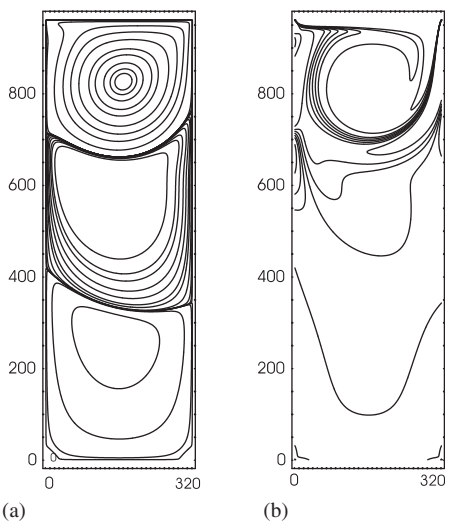

Figure 2. $Re = 1000$; A. ratio 3: $h_x = 1/320$, $h_y = 3/960$: (a) Streamlines; and (b) vorticity contours.

(3) a combination of mesh sizes and time steps, $(h_x, h_y) = (1/240, 3/720)$ with $\Delta t = 0.005$, $(h_x, h_y) = (1/320, 3/960)$ with $\Delta t = 0.0025$, and $(h_x, h_y) = (1/440, 3/1320)$ with $\Delta t = 0.00125$ (due to stability).

The discrepancies for each set of computations are:

(1) of microscopic order (at most $4 \times 10^{-7}\%$);
(2) at most 8% (0.9% for the stream function and 8% for vorticity);

(3) at most 9% (0.5% for the stream function and 9% for vorticity, the maximums occurring in the farthest, in size, meshes and time steps; for the close ones, the maximum is 5% for the vorticity).

Incidentally, the result with $(h_x, h_y) = (1/440, 3/1320)$ and $\Delta t = 0.00125$ mentioned in (3) was also computed with $\Delta t = 0.001$ giving a discrepancy like the one obtained in (1).

The max/min values of the stream function ψ (in all the cavity $\overline{\Omega}$) for cases (1) and (3) are displayed as follows ((2) is included in these two cases):

(1) max/min $= 0.0133/-0.1178$ (the same for all the Δt's);
(3a) $(h_x, h_y) = (1/240, 3/720)$ with $\Delta t = 0.005$, max/min $= 0.0135/-0.1189$,
(3b) $(h_x, h_y) = (1/320, 3/960)$ with $\Delta t = 0.0025$, max/min $= 0.0135/-0.1192$,
(3c) $(h_x, h_y) = (1/440, 3/1320)$ with $\Delta t = 0.00125$, max/min $= 0.0136/-0.1195$.

Therefore, the results shown in Figure 2 are chosen as the correct ones, which agrees with the one shown by $(h_x, h_y) = (1/440, 3/1320)$ and $\Delta t = 0.00125$. It is observed that the number of circles, 9, of the streamlines in the upper cell is very close to the Goyon [9] aspect ratio 2 result, 8 circles; because of the difference in aspect ratio, in such a Goyon result the third lower cell does not appear.

It is straightforward to verify the above study for the easier aspect ratio 2 result. Actually, computations were made on meshes $(h_x, h_y) = (1/240, 2/480)$, with $\Delta t = 0.005$, and $(h_x, h_y) = (1/320, 2/640)$, with $\Delta t = 0.0025$. The corresponding flows show 9 circles in the upper cell of the streamlines instead of 8, a in Figure 1; that is, a small circle appears in the centre of the cell; everything else looks the same, including the vorticity contours. However, the one on $(h_x, h_y) = (1/120, 2/240)$ and $\Delta t = 0.01$ is shown in Figure 1 to compare its agreement with Goyon's result on a mesh $(h_x, h_y) = (1/128, 2/256)$ (it also shows 8 circles in such cell).

It should be noted the increase in the correct meshes from the aspect ratio 2 result to the aspect ratio 3 case (from $(h_x, h_y) = (1/120, 2/240)$ to $(h_x, h_y) = (1/320, 3/960)$). Therefore, this and the stability constraint on the time step impose a serious limitation on computing resources either for higher aspect ratios or higher Reynolds numbers, at least under the current form of the numerical scheme.

4.2. Mixed convection thermal flows

The boundary condition for the temperature (given implicitly on the operator B, say in (12)) is given by

$$\frac{\partial \theta}{\partial n} = 0 \quad \text{on } \Gamma|_{x=0,a}; \quad \theta = \theta_0 \equiv 0 \quad \text{on } \Gamma|_{y=0}, \quad \theta = \theta_1 \equiv 1 \quad \text{on } \Gamma|_{y=b}$$

which means that the top wall is maintained at a higher temperature than the bottom wall and the lateral walls are insulated. Then, the fluid motion is caused by buoyancy from the vertical temperature gradient and by the velocity-driven cavity boundary condition on the top horizontal boundary wall.

Figures 3 and 4 show the flows for Reynolds number $Re = 1000$ and Grashof numbers $Gr = 10^2$ and $Gr = 10^6$ in the unit square cavity on a mesh $(h_x, h_y) = (1/120, 1/120)$, both with $\Delta t = 0.01$; the streamlines on the left are obtained with the contour values given by Ghia *et al.* [15] whereas the isotherms on the right are 'default' ones. Both results agree

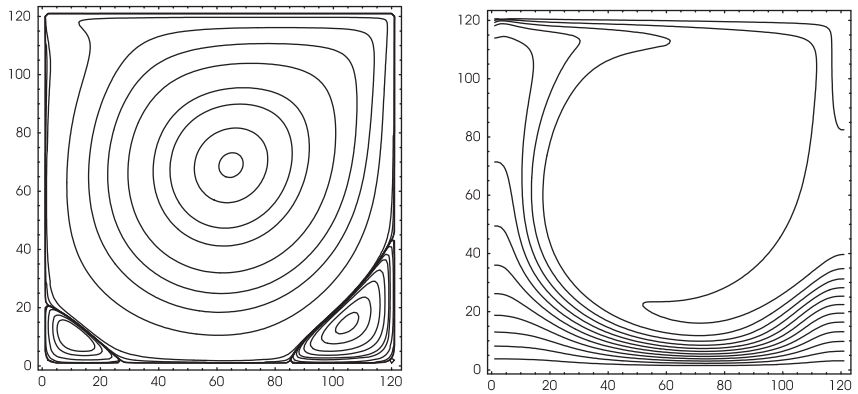

Figure 3. $Re = 1000$, $Gr = 10^2$; $h_x = 1/120 = h_y$: (a) Streamlines; and (b) vorticity contours.

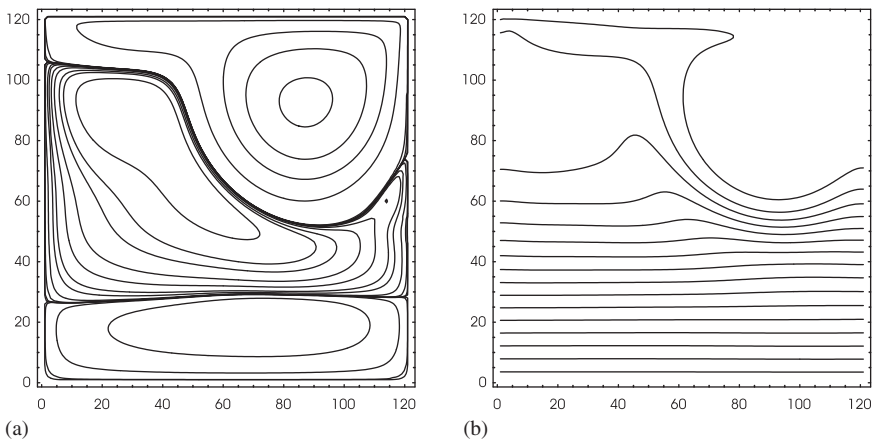

Figure 4. $Re = 1000$, $Gr = 10^6$; $h_x = 1/120 = h_y$: (a) Streamlines; and (b) isotherms.

with those in Reference [6]; they in turn were validated with the ones in Reference [14]. The validation from this work is reinforced by showing in Figure 5 the profiles of the horizontal U and vertical V component of the velocity at $x = 0.5$ (left) and $y = 0.5$ (right), respectively, for $Gr = 10^6$ fixed and $Re = 400$, 1000, 3000, with their min–max values given in Table I. All show good agreement with those reported by Iwatsu, Table II. The case $Re = 100$ (considered in Iwatsu) is skipped since it is a less difficult solution.

Figures 6 and 7 show the flows for Reynolds number $Re = 1000$ and Grashof number $Gr = 10^6$ with aspect ratios 2 and 3 on meshes $(h_x, h_y) = (1/120, 2/240)$ and $(h_x, h_y) = (1/120, 3/360)$, respectively, with $\Delta t = 0.01$; the streamlines, on the left, and the isotherms, on the right, are also obtained with the values mentioned for Figures 3 and 4.

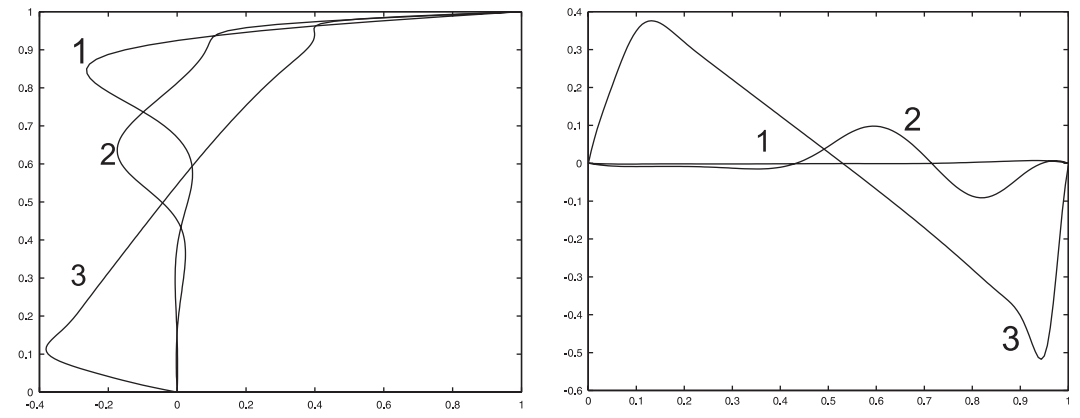

Figure 5. $Gr = 10^6$: (1) $Re = 400$, (2) $Re = 1000$, (3) $Re = 3000$.

Table I. $Gr = 10^6$: (1) $Re = 400$, (2) $Re = 1000$, (3) $Re = 3000$.

Velocity profiles	$U_{\min}$, $U_{\max}$	$V_{\min}$, $V_{\max}$
(1)	−0.2629, 0.9931	−0.0023, 0.0071
(2)	−0.1742, 0.9981	−0.0912, 0.0979
(3)	−0.3809, 0.9991	−0.5179, 0.3762

Table II. Iwatsu's results.

Velocity profiles	$U_{\min}$, $U_{\max}$	$V_{\min}$, $V_{\max}$
(1)	−0.26322627, 1.000000	−0.000897862948, 0.0072308369
(2)	−0.17038333, 1.000000	−0.0877381563, 0.0969309211
(3)	−0.40658975, 1.000000	−0.54972339, 0.40160173

To validate the aspect ratio 2 result, computations were made for a fixed mesh size and various time steps and *vice versa*:

(1) mesh size fixed, $(h_x, h_y) = (1/120, 2/240)$ and $\{\Delta t\} = \{0.02, 0.01, 0.005\}$;
(2) time step fixed, $\Delta t = 0.005$ and $\{(h_x, h_y)\} = \{(1/120, 2/240), (1/160, 2/320), (1/240, 2/480)\}$;
(3) a combination of time step and mesh size,
(3a) $\Delta t = 0.005$ with $(h_x, h_y) = (1/240, 2/480)$ and $\Delta t = 0.0025$ (due to stability) with $(h_x, h_y) = (1/320, 2/640)$,
(3b) $\Delta t = 0.01$ with $(h_x, h_y) = (1/120, 2/240)$ and $\Delta t = 0.0025$ with $(h_x, h_y) = (1/320, 2/640)$.

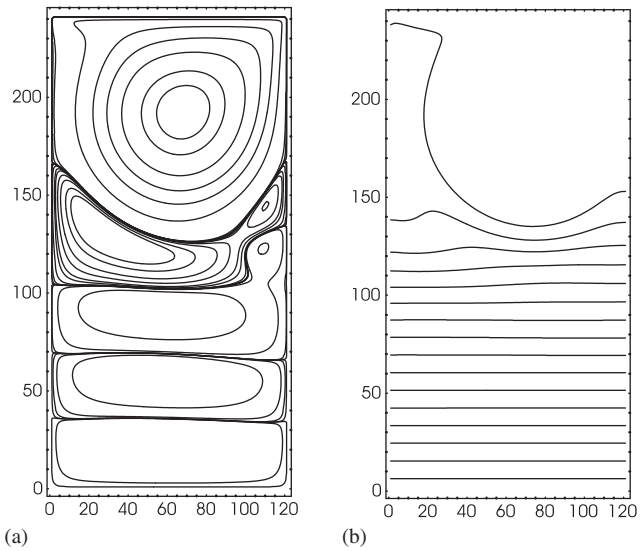

Figure 6. $Re = 1000$, $Gr = 10^6$; A. ratio 2: $h_x = 1/120$, $h_y = 2/240$: (a) Streamlines; and (b) isotherms.

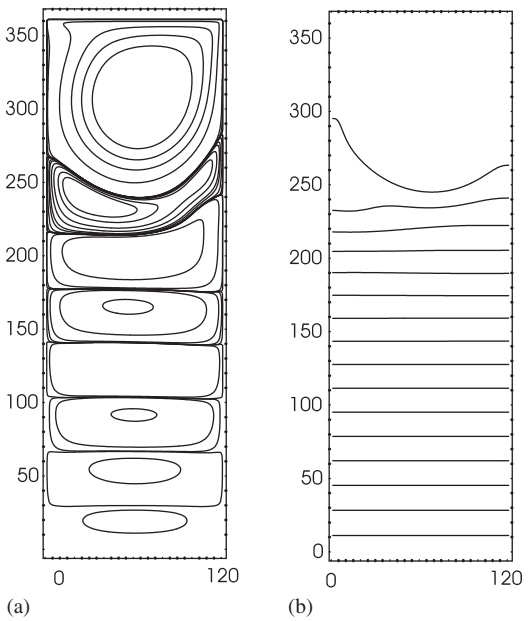

Figure 7. $Re = 1000$, $Gr = 10^6$; A. ratio 3: $h_x = 1/120$, $h_y = 3/360$: (a) Streamlines; and (b) isotherms.

Table III. Steady state times for mixed convection flows.

Gr	A. ratio	T_{ss}
(1) $Gr = 10^2$	1	107.65
(2) $Gr = 10^6$	1	372.97
(3) $Gr = 10^6$	2	1097.09
(4) $Gr = 10^6$	3	1511.41
(5) $Gr = 10^7$	1	430.26

The discrepancies from the above experiments are:

(1) at most 1.4% (this maximum occurs in the stream function for $\Delta t = 0.005$ and $\Delta t = 0.01$, the rest are less than 1%);
(2) at most 5% (5% for the stream function and 1% for temperature, these maximums occurring in the two farthest meshes);
(3a) at most 0.8% (0.8% for the stream function and 0.7% for temperature),
(3b) at most 3% (3% for the stream function and 0.6% for temperature).

It should be noted that in (3) the discrepancies are congruent with the mesh size.

The max/min values of the stream function ψ for (1)–(3) are:

(1) max/min $= 0.0027$ (same for all the Δt's)/-0.1069, -0.1067, -0.1066, respectively;
(2) $\Delta t = 0.005$ with $\{(h_x, h_y)\} = \{(1/120, 2/240), (1/160, 2/320), (1/240, 2/480)\}$, max/min $= 0.0027$ (same for all the meshes)/-0.1066, -0.01083, -0.1095, respectively;
(3) only $\Delta t = 0.0025$ with $(h_x, h_y) = (1/320, 2/640)$ since it can be compared with the previous ones in (1) and (2), max/min $= 0.0027/-0.1097$.

Then, because of the above minimal errors and since no changes are observed in figures with finer meshes, the flow shown in Figure 6, with $(h_x, h_y) = (1/120, 2/240)$ and $\Delta t = 0.01$, is taken as the correct one. As will be pointed out later, a thermal flow is more dynamic; hence it is notable that this result is obtained with a mesh that is analogous to one that works in the square cavity, Figure 4, that is, it happens something like in the isothermal case, Figure 1.

Concerning the aspect ratio 3 result shown in Figure 7, with $(h_x, h_y) = (1/120, 3/360)$ and $\Delta t = 0.01$, another computation was made with $(h_x, h_y) = (1/240, 3/720)$ and $\Delta t = 0.005$; the discrepancy between them is at most 3% (3% in the stream function and 0.2% in the temperature) and the figures look the same. Moreover, for the stream function the max/min $= 0.0025/-0.1134$ in both cases. At this stage, this result has to be taken as a preliminary one since more computing experiments need to be done to see if, for instance, some change in the streamlines like in the isothermal $Re = 1000$ aspect ratio 3 result, Figure 2, may occur. Unlike such an isothermal result, where the final time to reach the steady state is no more than $T_{ss} = 200$, the corresponding time for this thermal result is beyond $T_{ss} = 1000$ as shown in Table III and the discussion in Section 4.3. Hence, for finer meshes, and its time step restriction due to stability, considerable computing time is required.

Finally, Figure 8 shows the flow for Reynolds number $Re = 1000$ and Grashof number $Gr = 10^7$ in the unit driven cavity on a mesh $h_x = 1/120 \times 1/120 = h_y$: streamlines on the left and isotherms on the right with contour values like before. For this flow, experiments were

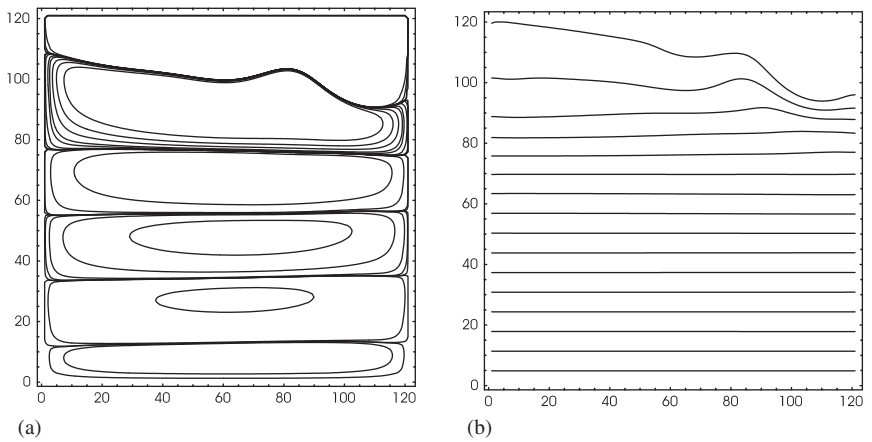

Figure 8. $Re = 1000$, $Gr = 10^7$; $h_x = 1/120 = h_y$: (a) Streamlines; and (b) isotherms.

computed as follows:

(1) fixed mesh size $(h_x, h_y) = (1/120, 1/120)$, $\{\Delta t\} = \{0.02, 0.01, 0.005\}$;
(2) a combination of three time steps and three mesh sizes,
(2a) $\Delta t = 0.01$ with $(h_x, h_y) = (1/120, 1/120)$ and $\Delta t = 0.005$ with $(h_x, h_y) = (1/240, 1/240)$,
(2b) $\Delta t = 0.01$ with $(h_x, h_y) = (1/120, 1/120)$ and $\Delta t = 0.00125$ (due to stability) with $(h_x, h_y) = (1/480, 1/480)$,
(2c) $\Delta t = 0.005$ with $(h_x, h_y) = (1/240, 1/240)$ and $\Delta t = 0.00125$ with $(h_x, h_y) = (1/480, 1/480)$.

The discrepancies are:

(1) at most 0.2% (0.2% for the stream function and 0.15% for temperature, these maximums occurring for the two farthest Δt's, the rest are almost of microscopic order);
(2a) at most of 3% (3% for stream function and 0.6% for temperature), almost the same occurs if $\Delta t = 0.01$ is replaced by $\Delta t = 0.005$ in the coarser mesh,
(2b) at most 3% (3% for stream function and 0.3% for temperature),
(2c) at most 0.5% (0.3% for stream function and 0.5% for temperature).

On the other hand, the max/min values of the stream function ψ in each case are:

(1) max/min $= 0.0057/0.0388$ (the same for all the Δt's);
(2c) max/min $= 0.0058/0.040$ (the same for both meshes). It should be noted that (2a)–(2b) are combinations of (1) and (2c).

Then, in terms of the above discrepancies and since no changes are observed in figures with finer meshes, the flow shown in Figure 8, with $(h_x, h_y) = (1/120, 1/120)$ and $\Delta t = 0.01$, is taken as the correct one.

Table III shows the final time T_{ss} where the asymptotic steady state is reached for mixed convection problems according to the point-wise discrete L_∞ absolute criterion in $\overline{\Omega}$

$$\omega : \|\omega^{n+1}_{hx,hy} - \omega^{n}_{hx,hy}\|_\infty, \quad \theta : \|\theta^{n+1}_{hx,hy} - \theta^{n}_{hx,hy}\|_\infty \tag{15}$$

with tolerance 10^{-5}. The Reynolds number $Re = 1000$ is fixed and the Grashof number Gr varies according to the flows in Figures 3, 4, 6–8.

Remark

The numerical experiments used for mesh size and time-step independence studies, based on (14), show that T_{ss} has some dependence on the time step and the mesh size: it decreases as either the time step or the mesh size decreases. To see if this may depend on the specific choice (15), experiments were also made with the discrete $L^2(\overline{\Omega})$ norm and a similar pattern is observed. Moreover, computations were made using the small T_{ss} for two analogous situations and (14) discrepancies on ψ and θ were computed: they are at most 5%; actually, for the same mesh and different time steps the differences are of microscopic order. Therefore, since the mesh size and time-step independence studies lead us to figure out the optimal mesh size and time step that give the correct results, it is reasonable to choose T_{ss} as the one occurring in such situations, which is shown in Table III in connection with Figures 3, 4, 6–8.

4.3. Some discussion on the results and the numerical procedure

About the new flows (Figures 2, 6–8), which to the best of our knowledge are reported for the first time, some specific facts can be pointed out. The number of cells for streamlines in the square cavity for mixed convection flows increases as the Grashof number grows: with $Re = 1000$ fixed, Figure 4, $Gr = 10^6$ has more cells than the one in Figure 3, $Gr = 100$, and less than the new one in Figure 8, $Gr = 10^7$; in rectangular cavities, this number of cells is also bigger than the one for isothermal flows, as can be seen comparing Figures 6 and 7 with Figures 1 and 2. From Table III it can be observed that the thermal flow needs more time to reach its asymptotic steady state T_{ss} as the aspect ratio or the Grashof number grows. Comparing the meshes for the results in Figures 3, 4, and 8 (square cavity) with the ones in Figures 2, 6, and 7, it follows that for high aspect ratios the mesh must be refined.

For the isothermal results of aspect ratio 2 and 3, the final time T_{ss} where the steady state is reached was determined in a different way: when the flow does not change any more. As in the thermal case, this time T_{ss} increases as the aspect ratio grows, but for the biggest aspect ratio considered here (3, with $Re = 1000$) this time is not greater than 200, then it is far smaller than the thermal cases; this and the bigger number of cells in the streamlines, discussed just above, may be seen as a result of mixed convection flows being more dynamic due to the double motion effect of their boundary condition, which is commented on after the θ boundary condition in (4.2).

At first it was supposed that, with this numerical scheme, it was going to be possible to resolve flows at high aspect ratios with an appropriate mesh, just taking as a guide the one that works in the square cavity. The mesh independence study leads one to conclude that this is not the case; finer meshes have to be used, which in turn gives rise to restrictions on the time step due to stability. The number of iterations at each time step starts at about 20–15 but it promptly decreases to 2–3, even 1, long before steady state is reached; this latter behaviour deteriorates when the time step starts to lose stability; at worst, it blows up immediately. It has also been observed, at least for isothermal flows in the square cavity, that such restrictions on the time step also appear for high Reynolds numbers once a fine mesh is used due to boundary layer effects. No systematic study has been carried out to see how

this trend is affected for different values of the parameter ρ in the iterative process. A value of $\rho = 0.7$ has been working effectively.

Moreover, to pass the non-symmetric (and non-linear due to the coupling through the velocity with vorticity and temperature) convection part of the elliptic operators to the right-hand side can be seen as an advantage of the iterative procedure. This process decouples equations and relies on linear problems. Keeping these forms on the left, an advantage could be to avoid iterations treating the non-linear convection terms as a linear extrapolation of the two preceding time values. This approach follows recent works in primitive variables, where the boundary condition is specified, for instance References [16, 17]. However, in the context of the 2D stream function–vorticity formulation, iterations are necessary to construct the boundary condition for vorticity in terms of unknown values of the stream function, (7) and (12)–(13).

5. CONCLUSIONS

2D isothermal/non-isothermal incompressible viscous flows in rectangular domains with various aspect ratios, in connection with the unregularized, driven cavity problem, have been presented. Results are shown for Reynolds number $Re = 1000$ in isothermal problems and for Reynolds number $400 \leqslant Re \leqslant 1000$ and Grashof numbers $10^2 \leqslant Gr \leqslant 10^7$ in mixed convection. The results are obtained with a simple numerical scheme based mainly on a fixed point iterative process to solve the non-linear elliptic systems that result after time discretization on the time-dependent Boussinesq and Navier–Stokes equations in stream function–vorticity variables. The numerical procedure leads to the solution of well-conditioned symmetric linear elliptic problems. With its simplicity, the procedure allows solutions to be obtained for flows, all of which reach their asymptotic steady state. From these results, regarding the mesh size and time step (a warning of it is given by the aspect ratio 3 result in Figure 2), it can be concluded that a study of flows at higher aspect ratios as well as of time-dependent flows at high Reynolds numbers (supposed to be so in connection with the square cavity for Reynolds numbers > 7500) could be unreachable, unless some additional improvement is made on the numerical scheme or through the use of more powerful computers.

ACKNOWLEDGEMENTS

We would like to thank the unknown reviewers for the careful reading of the manuscript and their remarks which have improved the presentation of this work.

REFERENCES

1. Nicolás A, Bermúdez B. 2D incompressible viscous flows at moderate and high Reynolds numbers. *Computer Modeling in Engineering and Sciences* 2004; **6**(5):441–451.
2. Foias C, Manley O, Rosa R, Teman R. *Navier-Stokes Equations and Turbulence.* Cambridge University Press, 2001.
3. Landau LD, Lifshitz EM. *Fluid Mechanics* (2nd edn). Pergamon Press: New York, 1989.
4. Mohammadi B, Pironneau O. *Analysis of the K-Epsilon Turbulence Model.* Wiley: New York, 1994.
5. Báez E, Bermúdez B, Nicolás A. Convección natural en medios porosos y libres: simulación numérica. *Revista Mexicana de Física* 2004; **50**(1):36–48.
6. Bermúdez B, Nicolás A. An operator splitting numerical scheme for thermal/isothermal incompressible viscous flows. *International Journal for Numerical Methods in Fluids* 1999; **29**:397–410.

7. Dean EJ, Glowinski R, Pironneau O. Iterative solution of the stream function–vorticity formulation of the Stokes problem, applications to the numerical simulation of incompressible viscous flow. *Computer Methods in Applied Mechanics and Engineering* 1991; **87**:117–155.
8. Peyret R, Taylor TD. *Computational Methods for Fluid Flow*. Springer: New York, 1983.
9. Goyon O. High-Reynolds number solutions of Navier–Stokes equations using incremental unknowns. *Computer Methods in Applied Mechanics and Engineering* 1996; **130**:319–335.
10. Gunzburger MD. *Finite Element Methods for Viscous Incompressible Flows*: *A Guide to Theory*, *Practice*, *and Algorithms*. Academic Press: New York, 1989.
11. Glowinki R. *Handbook of Numerical Analysis: Numerical Methods for Fluids* (Part 3). North-Holland: Amsterdam, 2003.
12. Adams J, Swarztrauber P, Sweet R. *FISHPAK*: *A Package of Fortran Subprograms for the Solution of Separable Elliptic PDE*'*s*. The National Center for Atmospheric Research: Boulder, CO, USA, 1980.
13. Sweet R. A cyclic reduction algorithm for solving block tridiagonal systems of arbitrary dimensions. *SIAM Journal on Numerical Analysis* 1977; **14**:706.
14. Iwatsu R, Hyn JM, Kuwahara K. Mixed convection in a driven cavity with a stable vertical temperature gradient. *International Journal of Heat Transfer* 1993; **36**:1601–1608.
15. Ghia U, Ghia KN, Shin CT. High-Re solutions for incompressible flow using the Navier–Stokes equations and a multigrid method. *Journal of Computational Physics* 1982; **48**:387–411.
16. Xin S, Le Quéré P. An extended Chebyshev pseudo-spectral benchmark for 8:1 differentially heated cavity. *International Journal for Numerical Methods in Fluids* 2002; **40**:981–998.
17. Badalassi VE, Ceniceros HD, Banerjee S. Computation of multiphase systems with phase field models. *Journal of Computational Physics* 2003; **190**:371–397.

